NASA/TM—2014-218332

The Effect of Experimental Variables on Industrial X-Ray Micro-Computed Sensitivity

Donald J. Roth
Glenn Research Center, Cleveland, Ohio

Richard W. Rauser
University of Toledo, Toledo, Ohio

December 2014

NASA STI Program . . . in Profile

Since its founding, NASA has been dedicated to the advancement of aeronautics and space science. The NASA Scientific and Technical Information (STI) program plays a key part in helping NASA maintain this important role.

The NASA STI Program operates under the auspices of the Agency Chief Information Officer. It collects, organizes, provides for archiving, and disseminates NASA's STI. The NASA STI program provides access to the NASA Aeronautics and Space Database and its public interface, the NASA Technical Reports Server, thus providing one of the largest collections of aeronautical and space science STI in the world. Results are published in both non-NASA channels and by NASA in the NASA STI Report Series, which includes the following report types:

- TECHNICAL PUBLICATION. Reports of completed research or a major significant phase of research that present the results of NASA programs and include extensive data or theoretical analysis. Includes compilations of significant scientific and technical data and information deemed to be of continuing reference value. NASA counterpart of peer-reviewed formal professional papers but has less stringent limitations on manuscript length and extent of graphic presentations.

- TECHNICAL MEMORANDUM. Scientific and technical findings that are preliminary or of specialized interest, e.g., quick release reports, working papers, and bibliographies that contain minimal annotation. Does not contain extensive analysis.

- CONTRACTOR REPORT. Scientific and technical findings by NASA-sponsored contractors and grantees.

- CONFERENCE PUBLICATION. Collected papers from scientific and technical conferences, symposia, seminars, or other meetings sponsored or cosponsored by NASA.

- SPECIAL PUBLICATION. Scientific, technical, or historical information from NASA programs, projects, and missions, often concerned with subjects having substantial public interest.

- TECHNICAL TRANSLATION. English-language translations of foreign scientific and technical material pertinent to NASA's mission.

Specialized services also include creating custom thesauri, building customized databases, organizing and publishing research results.

For more information about the NASA STI program, see the following:

- Access the NASA STI program home page at *http://www.sti.nasa.gov*

- E-mail your question to *help@sti.nasa.gov*

- Fax your question to the NASA STI Information Desk at 443–757–5803

- Phone the NASA STI Information Desk at 443–757–5802

- Write to:
  STI Information Desk
  NASA Center for AeroSpace Information
  7115 Standard Drive
  Hanover, MD 21076–1320

NASA/TM—2014-218332

The Effect of Experimental Variables on Industrial X-Ray Micro-Computed Sensitivity

Donald J. Roth
Glenn Research Center, Cleveland, Ohio

Richard W. Rauser
University of Toledo, Toledo, Ohio

National Aeronautics and
Space Administration

Glenn Research Center
Cleveland, Ohio 44135

December 2014

Trade names and trademarks are used in this report for identification only. Their usage does not constitute an official endorsement, either expressed or implied, by the National Aeronautics and Space Administration.

Level of Review: This material has been technically reviewed by technical management.

Available from

NASA Center for Aerospace Information
7115 Standard Drive
Hanover, MD 21076–1320

National Technical Information Service
5301 Shawnee Road
Alexandria, VA 22312

Available electronically at http://www.sti.nasa.gov

The Effect of Experimental Variables on Industrial X-Ray Micro-Computed Sensitivity

Donald J. Roth
National Aeronautics and Space Administration
Glenn Research Center
Cleveland, Ohio 44135

Richard W. Rauser
University of Toledo
Toledo, Ohio 43606

Abstract

A study was performed on the effect of experimental variables on radiographic sensitivity (image quality) in x-ray micro-computed tomography images for a high density thin wall metallic cylinder containing micro-EDM holes. Image quality was evaluated in terms of signal-to-noise ratio, flaw detectability, and feature sharpness. The variables included: day-to-day reproducibility, current, integration time, voltage, filtering, number of frame averages, number of projection views, beam width, effective object radius, binning, orientation of sample, acquisition angle range (180° to 360°), and directional versus transmission tube.

Background

Industrial X-ray Computed Tomography (CT) has become a critical nondestructive evaluation method in the last decade due to advances in detector, tube, and computational technology. These advancements have led to a range of applications for CT from the ability of CT to scan and reconstruct practically-sized (on the scale of 10s of centimeters and even meters) components at higher resolutions and higher speeds, as well as to perform materials characterization at the sub-1 μm level (Refs. 1 to 5).

Radiographic sensitivity is the size of the smallest detail that can be seen in a radiograph or the ease with which small details can be detected. Sensitivity depends on the sharpness and the contrast of the resulting image. Several figures of merit related to CT system sensitivity are available. Equation (1) shows an estimate of the signal-to-noise ratio (SNR) in a voxel element as a function of various CT system characteristics/experimental variables for a reconstruction of a cylindrical object (Refs. 6 and 7):

$$SNR = 0.665\mu w^{1.5}\sqrt{\frac{nvqt}{\Delta p}\exp(-2\pi R)} \tag{1}$$

where μ is the linear attenuation coefficient, w is the x-ray beam width, v is the number of projection views, n is the number of frame averages, q is the photon intensity rate at the detector, t is the integration time of the detectors, Δp is the ray spacing and R is the radius of the object. The number of frame averages (n) has been incorporated by the authors into the original equation found in (Ref. 6) since SNR is proportional to the square root of the number of frame averages. SNR increases as x-ray beam width, number of views, x-ray beam intensity, number of frame averages, and integration time increases. (Additionally, as the number of views increases, the ability to more precisely reconstruct the object increases (Ref. 7).) SNR also increases as ray spacing and object radius decreases. The photon intensity rate q will increase with increasing source voltage and / or current as more electrons per unit time bombard the target and subsequently produce more photons per unit time. Not indicated by Equation (1) but necessary to mention is that limiting/collimating the x-ray beam to a fan beam the height of one row of detector pixels, and increasing detector pixel size, also increase SNR.

Several variables can be used to experimentally and quantitatively assess x-ray and CT image quality. The first one, SNR, is experimentally measured in a digital image by dividing the mean gray level by the standard deviation (σ) in a representative area of the image so that the effect of these variables can be measured.

$$SNR = \frac{\text{mean}}{\sigma} \tag{2}$$

Another parameter, contrast ratio (*CR*), is given by (Ref. 7):

$$CR = \frac{6}{\sqrt{SNR * Z}} \tag{3}$$

where *Z* is the number of pixels over which the contrast is observed. Equation (3) shows that the larger the SNR and the greater the number of pixels over which contrast is observed, the lower (better) the contrast ratio that can be achieved. Computed tomographic systems often provide contrast sensitivity measurements on the order of 0.1 to 1.0 percent (Ref. 7). Using the measured SNR and knowing the number of pixels in the area over which SNR was measured, CR can also be determined experimentally.

Related to SNR and CR, contrast-to-noise (CNR) ratio is a potential figure of merit for assessing flaw detectability in a CT image when the flaw presents a gray scale variation from the background of the image. Figure 1 illustrates the definitions for signal contrast (C) and noise (N) (Ref. 8). Signal contrast can be defined as the difference between the mean gray level in the line drawn through the center of the flaw (M) and the minimum gray level in the flaw area (maximum dip gray value) (d_{max}). Noise can be defined as the difference between M and the minimum gray value on either side of the flaw. CNR is then obtained from:

$$CNR = \frac{C}{N}. \tag{4}$$

Scatter from the object itself as well as external sources can add a background haze (noise) to radiation intensities so that the CNR is reduced.

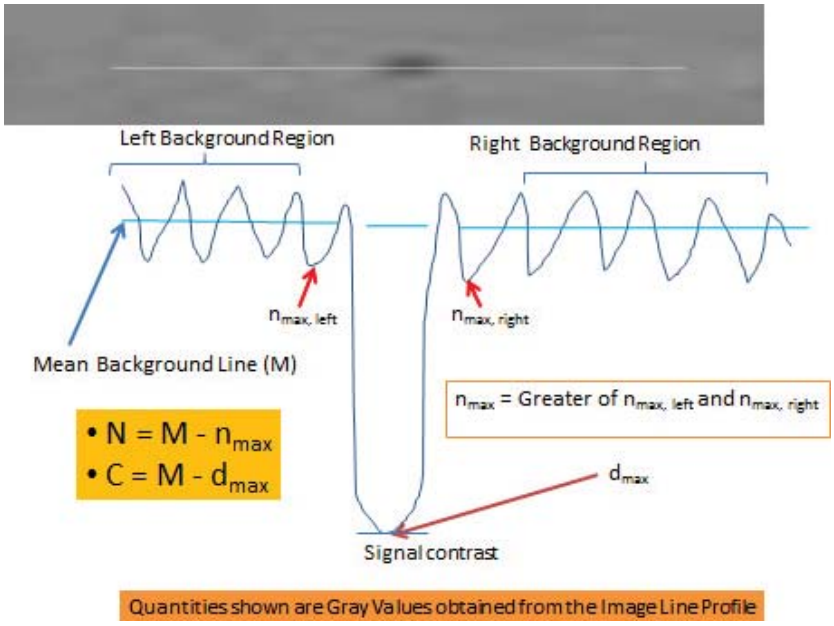

Figure 1.—Definitions for signal contrast (C) and noise (N).

Variables affecting SNR would be expected to have a similar effect on CNR. CNR, although desired as a measurement for probability of detection (POD) studies (Ref. 8), is problematic to implement for very small flaws covering a limited number of pixels. It requires a line profile to be drawn directly through the center of the indication, and the ability to discern where the flaw indication ends and noise begins. Incorrect line draws, even by one pixel, can cause dramatic error in calculation of CNR. One cumbersome way to overcome this is to draw many lines at different angles and obtain average values for contrast and noise, but this was not feasible for this investigation.

In this study, SNR is used to quantitatively assess the effect of variables on CT image quality. Qualitative evaluations of cylinder wall sharpness and detectability of the most difficult-to-detect hole are also utilized for assessing image quality. (A quantitative measure of sharpness can also be obtained in the following manner. A line profile of an edge can be differentiated and Fourier-transformed to obtain modulation transfer function (Ref. 7), but this is beyond the scope of this article.). The variables to be evaluated for effect on image quality include day-to-day reproducibility, current, integration time, voltage, filtering, number of frame averages, number of projection views, beam width, effective object radius, binning, orientation of sample, angle range (180° to 360°), and directional versus transmission tube.

CT Inspection Tradeoffs

Tradeoffs are often required in performing inspections with CT and because they affect SNR, are mentioned here. For example

- The greater the integration time (or lower number of frames per second) and the higher the number of frame averages, both of which improve SNR, the more time is required for the CT scan.
- Larger detector element size increases SNR but reduces resolution and accuracy of representing an indication (Ref. 7).
- Beam collimation to a fan beam the height of one row of detector pixels increases SNR over cone beam CT but increases scan time to obtain a full-height image.
- Increased beam width increases SNR according to Equation (1), but would be expected to reduce sensitivity as the ratio of the beam width to lateral flaw size increases.
- The effective radius R that the detector sees is decreased as the object moves closer to the detector for an object smaller than the detector. This is expected to increase SNR according to Equation (1), but will increase voxel dimension and thus reduce resolution [while also reducing geometric unsharpness] (the latter is less of an issue at very small focal spots).
- Increased photon intensity rate via increased voltage and / or current increases SNR but increased voltage will also decrease contrast between different phases and thicknesses in a material as higher energy x-rays more similarly penetrate the different phases and thicknesses than less energetic x-rays (increased latitude). Additionally, increased voltage and current result in more power and a larger focal spot size to prevent the target from overheating. A larger focal spot decreases sensitivity.

CT System and General Procedure

Microfocus x-ray Computed Tomography (μCT) is a non-destructive imaging technique designed to inspect complex-shaped parts for micron scale or larger flaws. Multiple x-ray projection images are acquired, followed by software reconstruction techniques using the projection images, to obtain cross-sectional slices of the part. The cross-sectional images can be viewed individually or used to render a volume. Two X-ray WorX microfocus sources that produce a cone beam were used in this study. These were the XWT-225-THE 225 keV transmission tube (< 5 μm spot size at lowest powers, 25 W power)

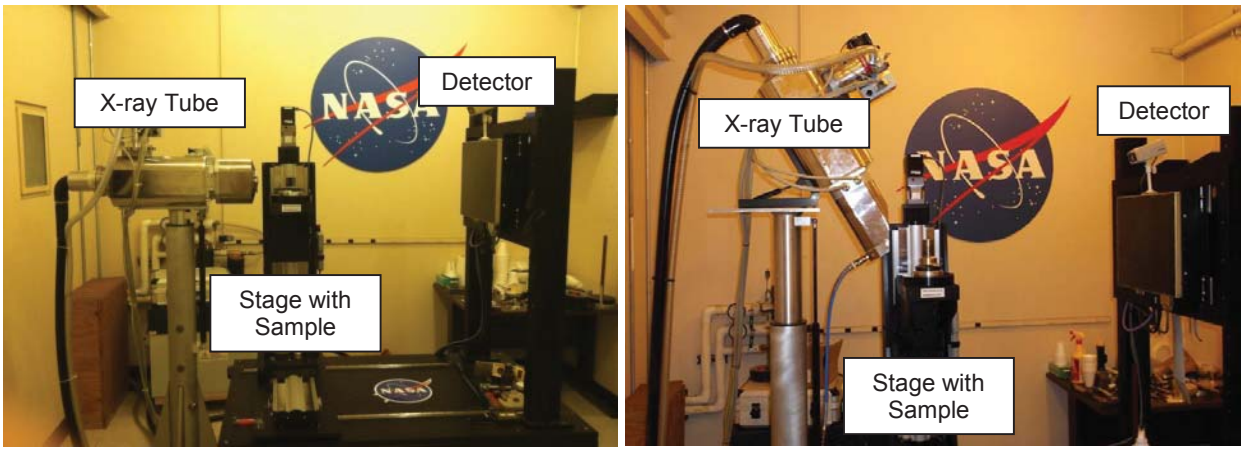

(a) (b)

Figure 2.—NASA Glenn Research Center X-ray CT system hardware. (a) Shown with transmission tube. (b) Shown with reflection/directional tube.

and the X-ray WorX SE-225 225 keV reflection/directional tube (< 5 μm spot size at lowest powers, 300 W power). The detector is a Dexela 2923 (true 14-bit dynamic range, 0.0748-mm pitch, 29- by 23-cm area, and 3888×3072 pixel elements). This detector has nearly half of the pixel pitch of the commercial grade prior state-of-the-art detectors utilized for microfocus digital x-ray (typically 0.127 mm). The acquisition, reconstruction, and visualization software is from Northstar Imaging, Inc. (NSI). Four-axis motion control allows automated positioning and scanning. The system, shown in Figure 2, has resolution capability easily > 30 line pair/mm.

Prior to the experiments, the sample stage and detector were precision-leveled, and detector and geometric calibrations were performed for every scan. CT scans were performed with the long axis of the cylindrical part aligned vertically. All CT scans were accomplished over the full 360° except for the limited angle range experiments. A procedure to reduce unsharpness was accomplished prior to reconstruction using a software algorithm in the NSI software. Subsequently, fast Feldkamp (FDK) reconstruction was performed on the projection view data set (Ref. 9).

Sample

The cylinder sample was made of MarM 247 nickel-based superalloy with wall thickness ~ 300 μm. A micro-EDM procedure was performed to create a pattern of holes of varying diameter and depth (see Figure 3). The most difficult-to-detect hole examined in this investigation was 32 μm in diameter and 50 μm in depth. The detectability of this hole was used to qualitatively assess CT image quality. (Diameters and depths were obtained by SEM and optical characterization, respectively, with an estimated uncertainty of ±10 percent).

Analysis Methodology

Flaw detection in top views of cylindrical CT data is very difficult if the walls of the cylinder are very thin. It can be advantageous to unwrap and reslice the 360° data so as to view two-dimensional “sheets” from the exterior to interior of the cylinder separated by the voxel dimension. The data analysis in this study was performed on sections of unwrapped/resliced CT images for two of the three measures. The

unwrapping and reslicing of the top view slice set was done using NASA CT-CURS software (Ref. 1). A precision alignment procedure of the top view slice set is required to obtain best results and is included as part of the unwrap/reslice software procedure. The unwrapped reslice images were automatically contrast expanded between the minimum and maximum gray level values as part of the software procedure. *The latter procedure will likely impact the subjective assessment of effect of variables on contrast versus analysis with images that all have a gray level between the same minimum and maximum. However, it was required to perform this procedure in order to characterize the most difficult-to-detect flaw.*

The unwrapped/reslice used for flaw detectability assessment and SNR determination was either the brightest and/or highest resolution of the series of unwrapped images in a data set. For SNR determination, an area just to the left the flaws shown in Figure 3 of at least 8000 to 10000 pixels was analyzed. The area analyzed for SNR was pure background—it did not contain any of the micro EDM holes. Screen captures of the most difficult-to-detect hole from the unwrapped/reslice image and of a wall area from a top (plan) view slice at the middle of the stack were obtained and compared within each series of experiments.

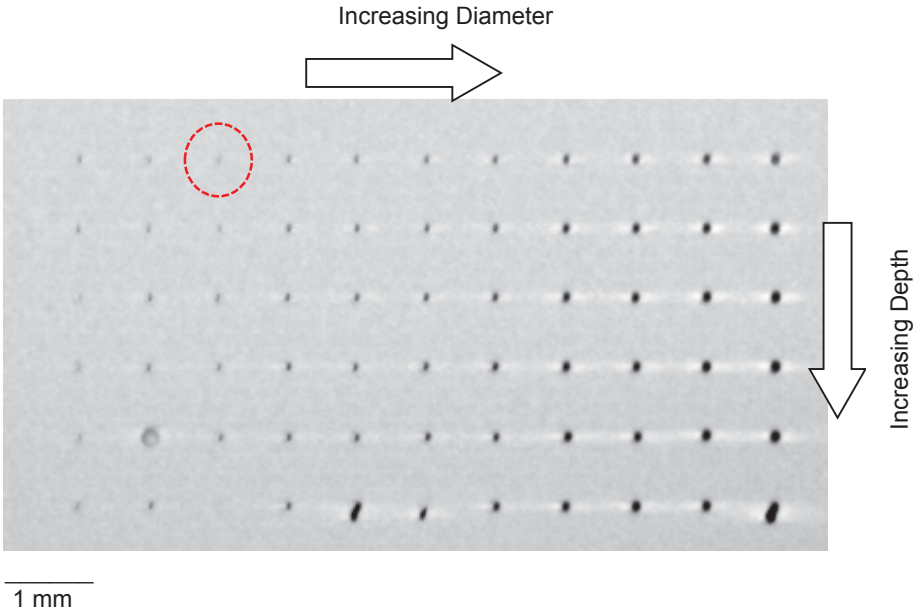

Figure 3.—Micro-EDM hole pattern (unwrapped-resliced CT view) in thin wall section near outer diameter surface. Hole circled was the most difficult to detect hole in the pattern.

Experiments and Results

The tables below lists the experiments and range of these parameters studied. Photon counts at the detector were adjusted using current and frame rate so that mean counts value with no sample present was kept at 60 to 70 percent of the detector's saturation limit of 16,384 (except for variables of current and frame rate (integration time) which directly affect photon count).

Day-to-Day Reproducibility (Reflection/Directional Tube)

CT scans were performed under nearly identical conditions given in Table 1 three days in a row, separated by ~ 24 hr.

Day 1 showed a lower SNR and the hole was subsequently more difficult to detect than for days 2 and 3 (see Table 2). It is likely that detector photon count at the detector was lower in day 1 versus days 2 and 3. Inner cylinder wall was well-defined each day. *Subsequent series of experiments where puzzling or unexpected results were observed were run at least twice to assure consistent results.*

TABLE 1.—EXPERIMENTAL PARAMETERS FOR DAY-TO-DAY REPRODUCIBILITY EXPERIMENTS

Parameter	Value
Reproducibility	Day 1 to 3
Voltage, kV	170
Current, μA	130
Estimated approximate focal spot, μm	10
Binning	1×1
Frame rate, frames per second (fps)	3
Number of frame averages	3
Filtering	0.16 in. Cu
Number of projection views	1800
Magnification factor	6.62
Voxel dimension, μm	11.3

TABLE 2.—RESULTS FOR DAY-TO-DAY REPRODUCIBILITY

[The scale bar shown in the top row images is approximately the same for all images from this point forward in the manuscript.]

Day	SNR	Hole	Wall
1	23.4	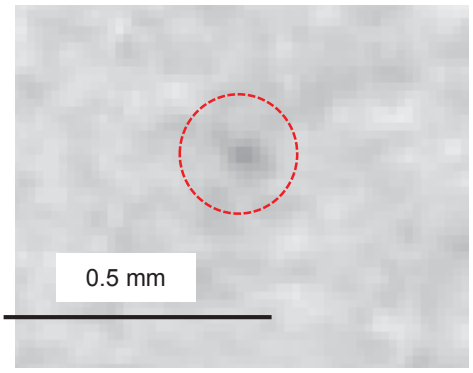 Circled area shows hole	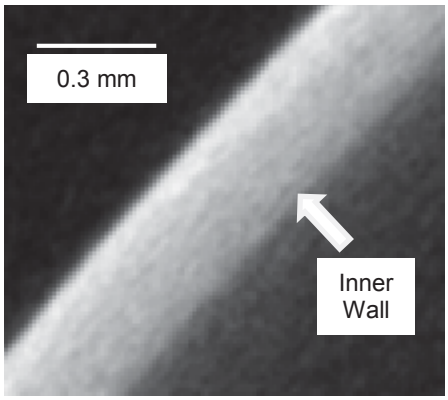
2	30	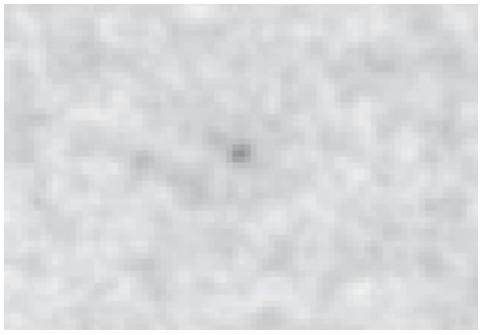	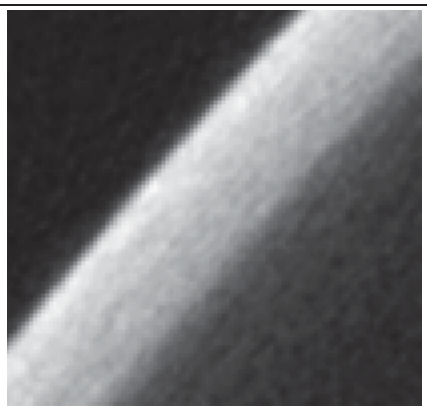
3	29.5	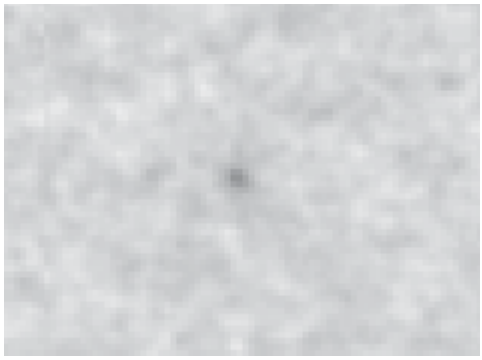	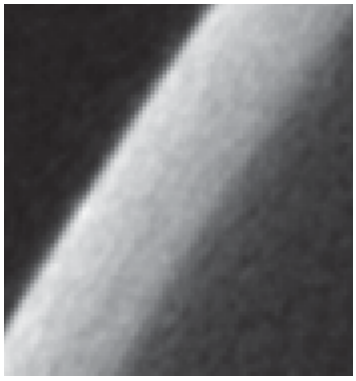

Varying Voltage and Filtering (Transmission Tube)

All else being equal, the effect of increasing voltage (energy) in digital radiography is to increase penetration (Ref. 7). The effect of increasing voltage in combination with applying more beam hardening filtration increases latitude (the thickness range of inspection possible). The effect of decreasing voltage is generally greater contrast between discontinuities and background material as lower energy radiation is preferentially attenuated by thicker and / or more dense sections.

Five basic voltages were utilized while keeping filtering constant using three different filters (Table 3). Current and integration time were adjusted to keep photon count through the sample at the detector within 10 percent for the different voltages. The steel and Cu filters were close in terms of radiographic equivalence and would be expected to yield similar results. (1.6 * 0.16 in. Cu = 0.26 in. Steel where 1.6 is the radiographic equivalence filtering factor for Cu at 150 kV as compared to Steel.)

Only the results for 210, 170, and 130 kV are shown regarding the effect of filtering in Table 4 to Table 6.

At 210 kV and using these filters, SNR is similar, the hole is detectable, and the inner cylinder wall is defined for these trials with poorest wall definition using the 0.24 in. steel filter.

TABLE 3.—EXPERIMENTAL PARAMETERS RELATED TO VARYING FILTERING WHILE KEEPING VOLTAGE CONSTANT AND VARYING VOLTAGE WHILE KEEPING FILTERING CONSTANT
[All other experimental parameters were the same as shown in Table 1.]

Voltage, kV	Filter	[a]Current/frame rate, µA/fps
210	0.16 in. Cu 0.24 in. Steel 0.028 in. Pb	110 / 3
190	0.16 in. Cu 0.24 in. Steel 0.028 in. Pb	120 / 3
170	0.16 in. Cu 0.24 in. Steel 0.028 in. Pb	130 / 3
150	0.16 in. Cu 0.24 in. Steel 0.028 in. Pb	150 / 3
130	0.16 in. Cu 0.24 in. Steel 0.028 in. Pb	185 / 2

[a]Current (µA) and / or frame per second (fps) value adjusted to keep photon count through the sample at the detector within 10 percent for the different voltages.

TABLE 4.—RESULTS FOR EFFECT OF FILTERING WITH 210 kV VOLTAGE

Voltage kV	Filter	SNR	Hole	Wall
210	0.16 in. Cu	23		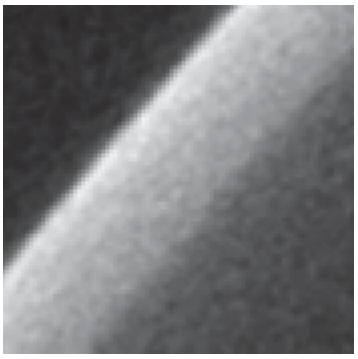
210	0.24 in. Steel	21.8	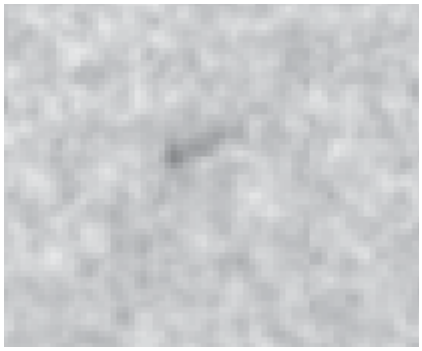	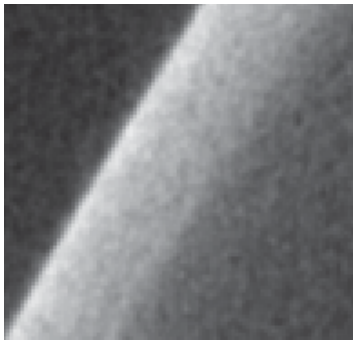
210	0.028 in. Pb	22	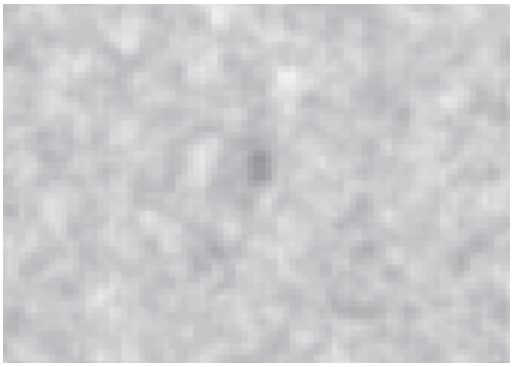	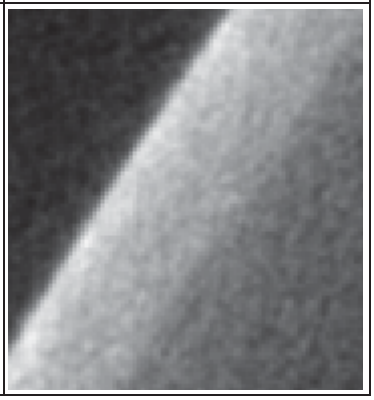

TABLE 5.—RESULTS FOR EFFECT OF FILTERING WITH 170 kV VOLTAGE

Voltage, kV	Filter	SNR	Hole	Wall
170	0.16 in. Cu	29		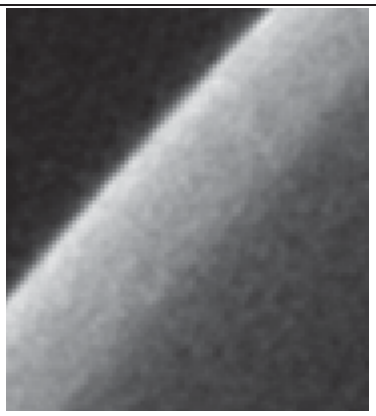
170	0.24 in. Steel	24	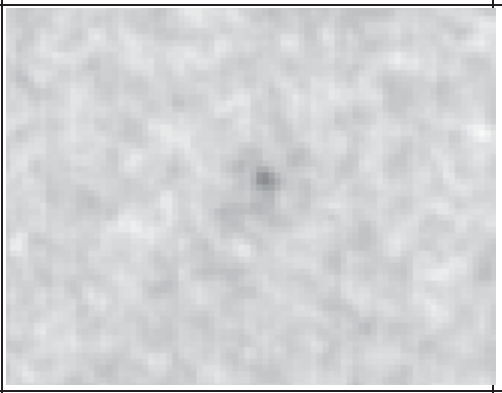	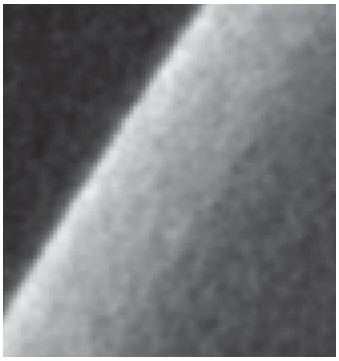
170	0.028 in. Pb	19.9	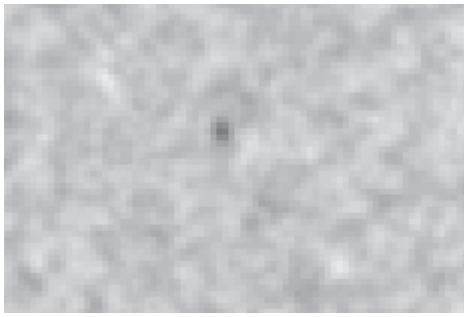	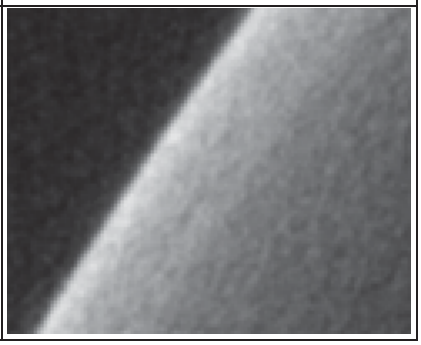

At 170 kV and using these filters, SNR is significantly different, the hole is detectable, and the inner cylinder wall is most well-defined using the 0.16 in. Cu filter.

TABLE 6.—RESULTS FOR EFFECT OF FILTERING WITH 130 kV VOLTAGE

Voltage, kV	Filter	SNR	Hole	Wall
130	0.16 in. Cu	27	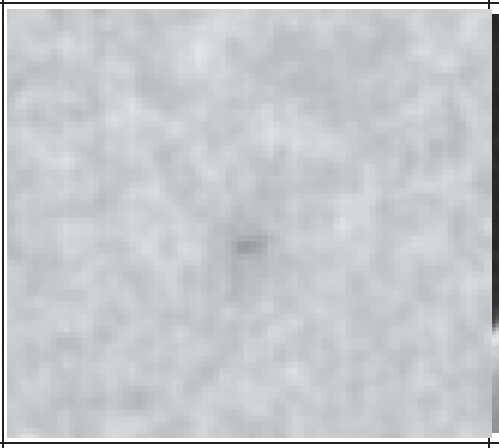	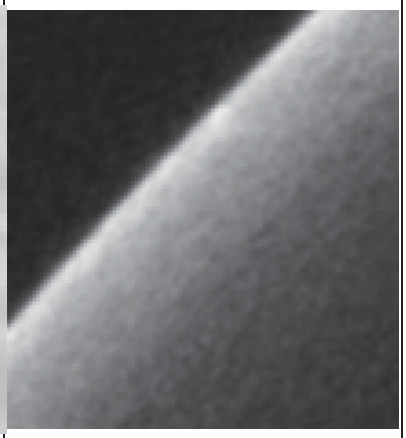
130	0.24 in. Steel	26	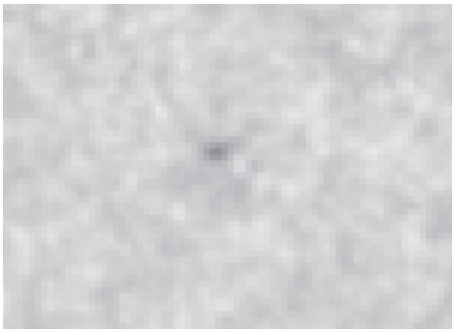	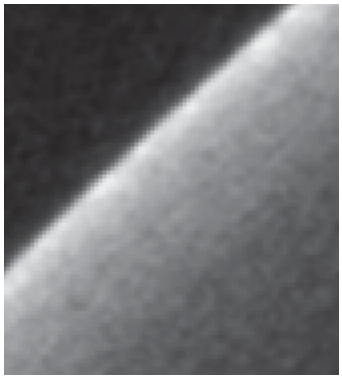
130	0.028 in. Pb	35	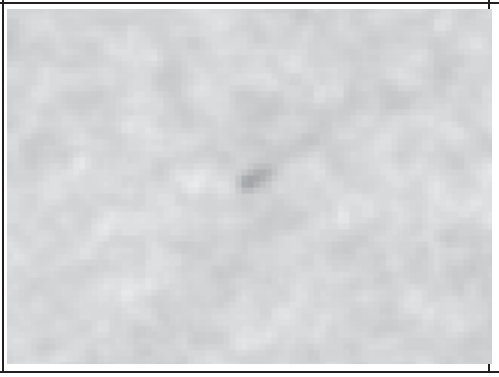	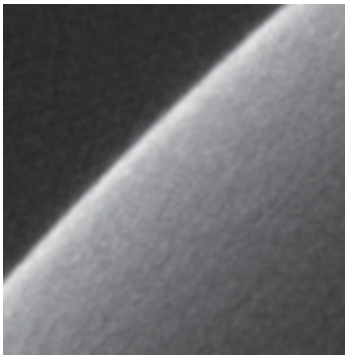

At 130 kV and using these filters, SNR is similar for Cu and steel filters, the hole is detectable, and the inner cylinder wall is ill-defined in all cases.

Table 7 reorganizes data to show the effect of voltage using the 0.16 in. Cu filter.

SNR did not follow a defined trend as the voltage decreased which was unexpected. The hole is detectable for all voltages but inner cylinder wall clearly becomes more well-defined as voltage is increased due to a reduction in scatter and increased latitude.

TABLE 7.—RESULTS FOR EFFECT OF VOLTAGE WITH 0.16 in. Cu FILTER

Voltage, kV	SNR	Hole	Wall
210	23		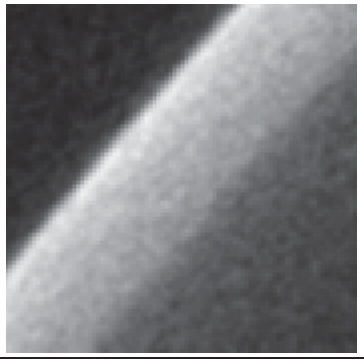
190	25.4	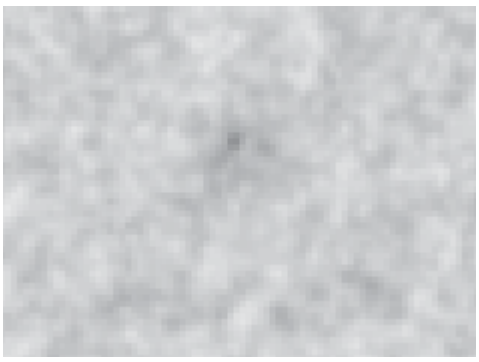	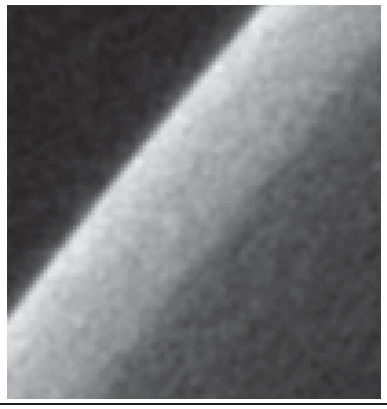
170	29		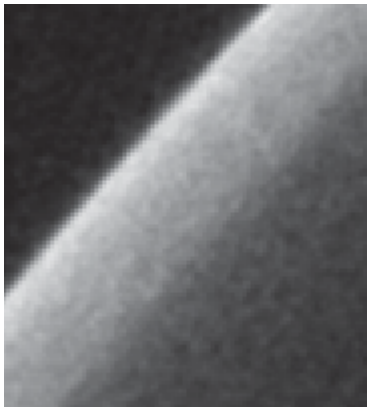

TABLE 8.—CONCLUDED

Voltage, kV	SNR	Hole	Wall
150	27	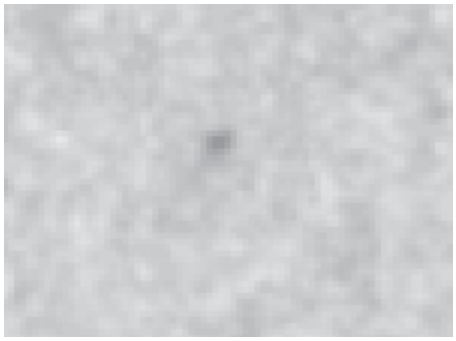	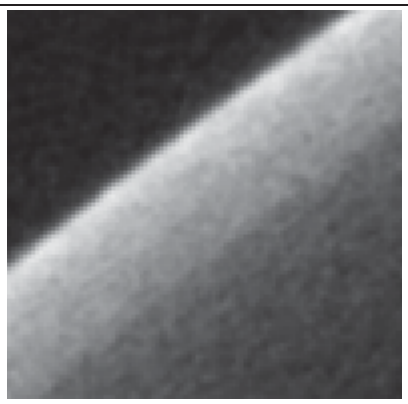
130	27	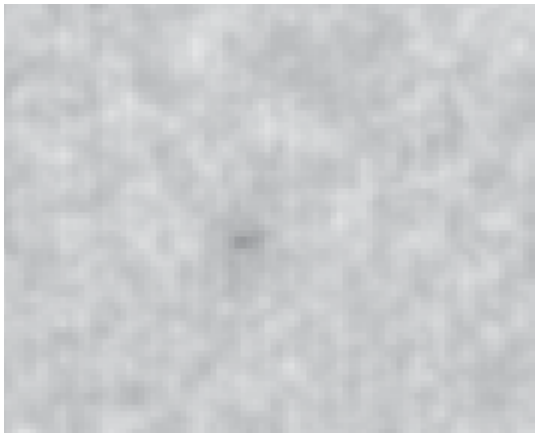	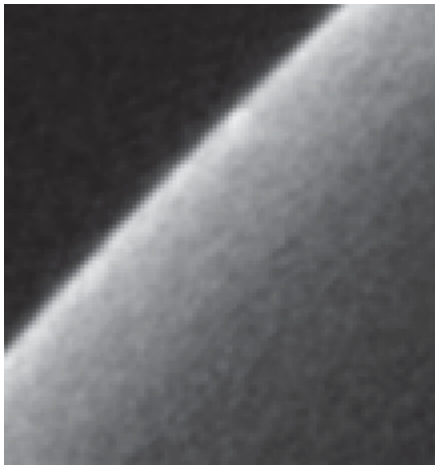

Varying Voltage and Filtering (Reflection/Directional Tube)

The set of experiments described by the parameters of Table 3 for the transmission tube was repeated for the reflection / directional tube and the results are shown in Table 8.

As for the transmission tube, SNR did not follow a defined trend as the voltage decreased. The hole is detectable for all voltages but the inner cylinder wall clearly becomes more well-defined as voltage is increased above 130 kV due to a reduction in scatter. The inner wall appears to be more highly resolved at most voltages for the reflection tube versus transmission tube. This may be due to a higher respective photon flux during the reflection tube experiments. However, Figure 4 shows nearly identical top view section CT image results for Transmission versus Reflection tube at 170 kV.

TABLE 9.—RESULTS FOR EFFECT OF VOLTAGE WITH 0.16 in. Cu FILTER

Voltage	SNR	Hole	Wall
210	28	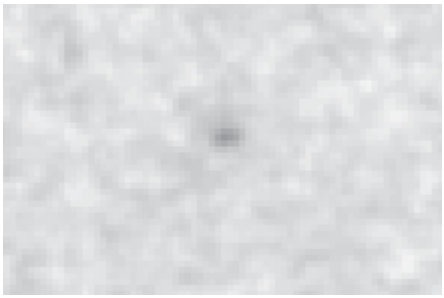	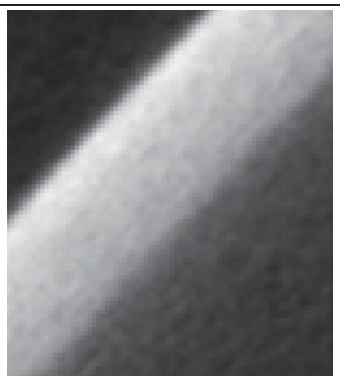
190	30.5	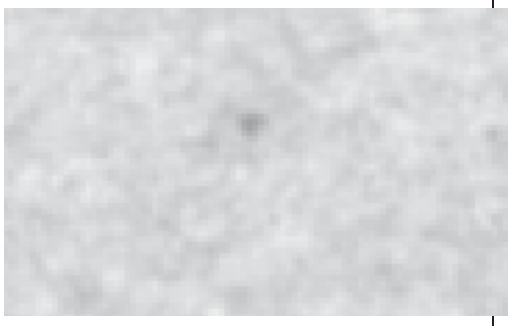	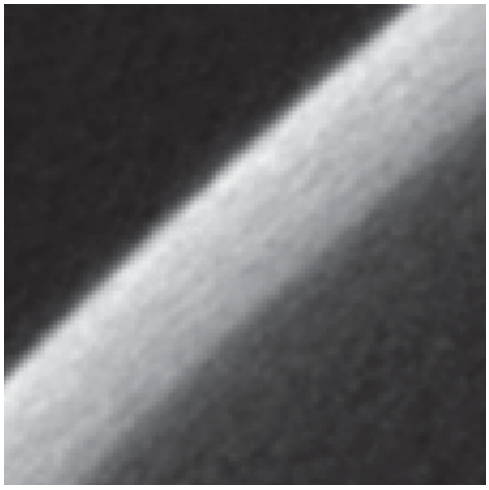

TABLE 8.—CONCLUDED

Voltage	SNR	Hole	Wall
170	28	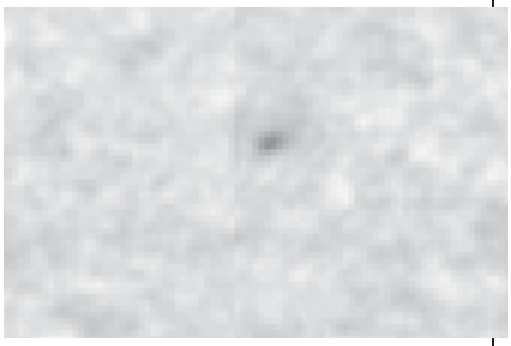	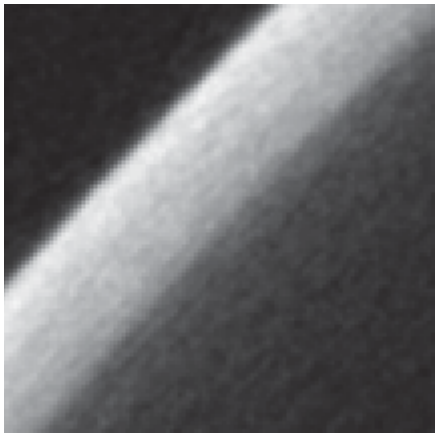
150	28	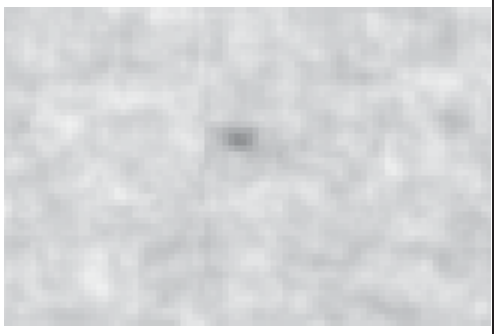	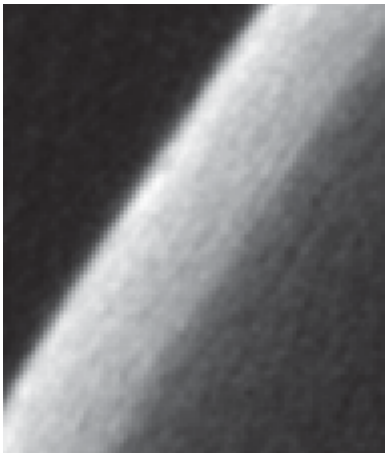
130	25.5		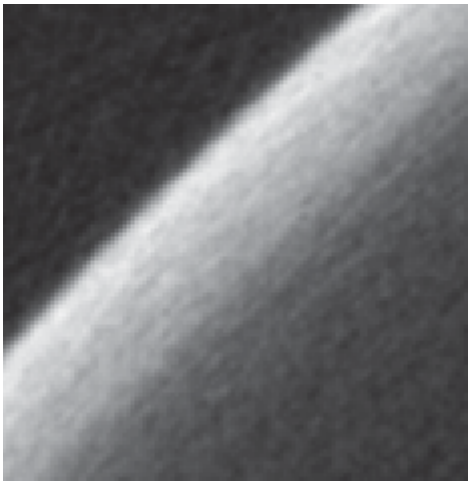

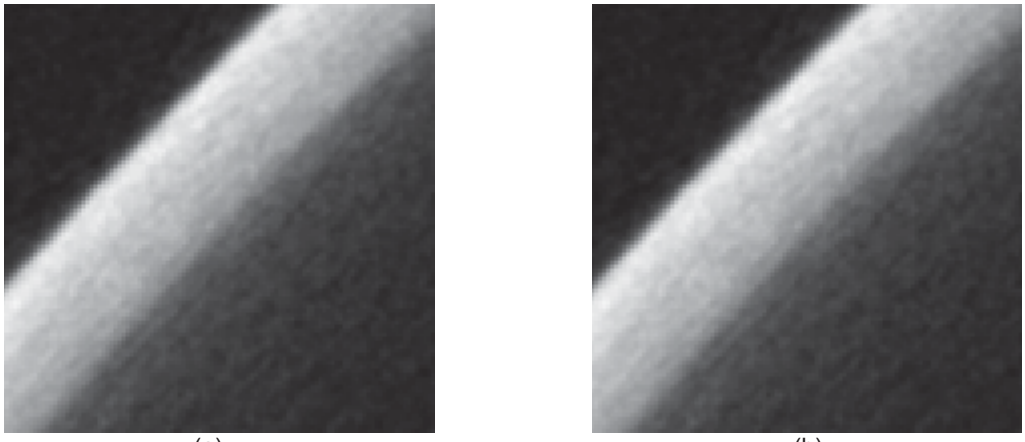

(a) (b)

Figure 4.—Top view section CT image at 170 kV for (a) transmission tube and (b) reflection tube.

TABLE 10.—EXPERIMENTAL PARAMETERS FOR EFFECT OF FRAME AVERAGING EXPERIMENTS

Parameter	Value
Frame averaging	1, 3, 5, 9, 15
Voltage, kV	70
Current, μA	200
Estimated approximate focal spot, μm	7
Binning	1×1
Frame rate, fps	3
Filtering	0.010 in. Cu
Number of projection views	360
Magnification factor	6.62
Voxel dimension, μm	11.3

Varying the Number of Frame Averages (Transmission Tube)

The effect of frame averaging is pronounced (see Table 9 for parameters and Table 10 for results). SNR increases significantly with increased frame averaging, as predicted by Equation (1), and both the hole and *outer* wall images are sharper. The inner cylinder wall is not resolved at 70 kV voltage. Similar sharpness increase would be expected with increasing number of views for the inner wall for CT scans run at higher voltages such as 190 kV.

TABLE 11.—RESULTS FOR EFFECT OF FRAME AVERAGING

No. of frame averages	SNR	Hole	Wall
1	10	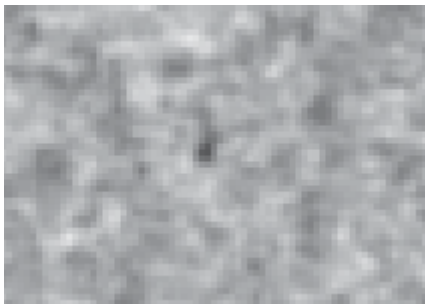	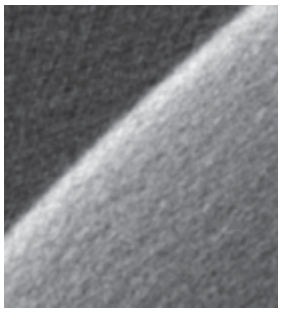
3	16.5	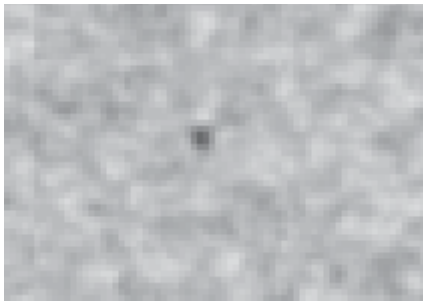	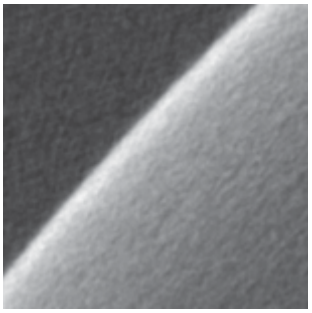
9	22.5	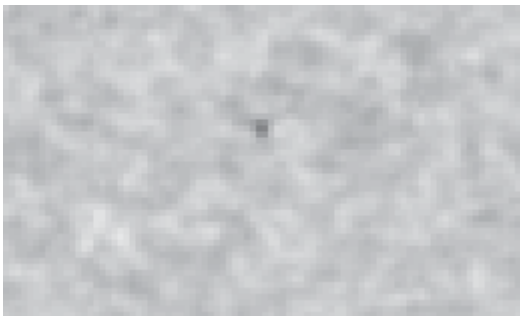	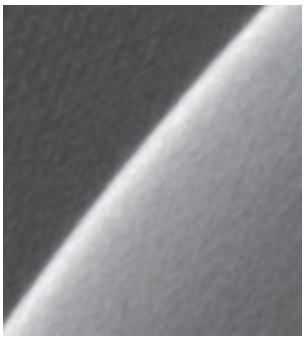
15	28.5	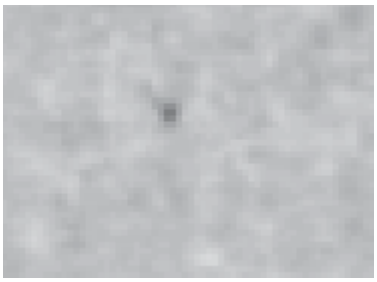	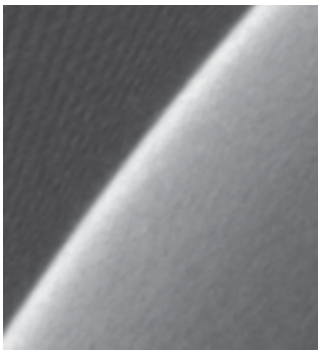

Varying the Number of Projection Views (Transmission Tube)

SNR increases with an increase in the number of projection views, as predicted by Equation (1) (see experiment parameters in Table 11). Detectability of the hole is reduced with a decrease in the number of projection views below 360. The inner cylinder wall is not resolved at 70 kV but the *outer* wall definition appears sharper with an increase in the number of projection views (see Table 12). Similar sharpness increase would be expected with increasing number of views for the inner wall for CT scans run at higher voltages such as 190 kV.

TABLE 12.—EXPERIMENTAL PARAMETERS FOR EFFECT OF NUMBER OF PROJECTION VIEWS EXPERIMENTS

Parameter	Value
Number of views	9, 18, 36, 90, 180, 360, 720, 1080, 1440, 1800
Voltage, kV	70
Current, μA	200
Estimated approximate focal spot, μm	7
Binning	1×1
Frame rate, fps	3
Number of frame averages	3
Filtering	0.010 in. Cu
Magnification factor	6.62
Voxel dimension, μm	11.3

TABLE 13.—RESULTS FOR EFFECT OF NUMBER OF PROJECTION VIEWS

No. of projection views	SNR	Hole	Wall
9	6 (analysis included striping in image)	A number of holes resolved but most difficult-to-detect hole not detected	Entire top view slice. Aliasing lines clearly visible. 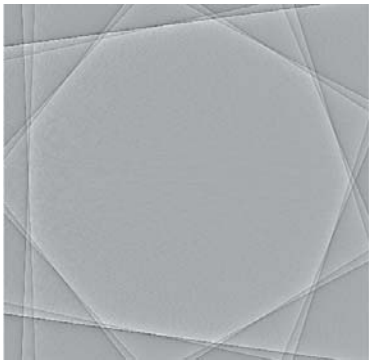

TABLE 12.—CONTINUNED

No. of projection views	SNR	Hole	Wall
18	11	A number of holes resolved but most difficult-to-detect hole not detected	Entire top view slice. Aliasing lines clearly visible. 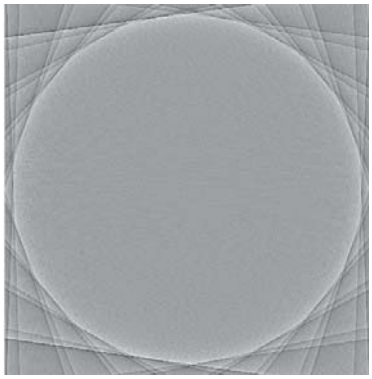
36	19	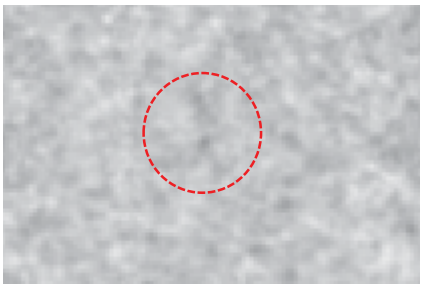 Hole barely detected	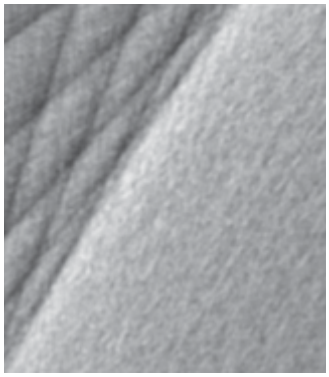
90	22.5	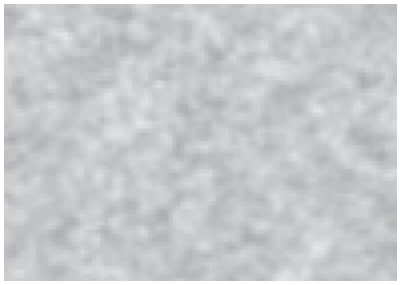 Hole not detected	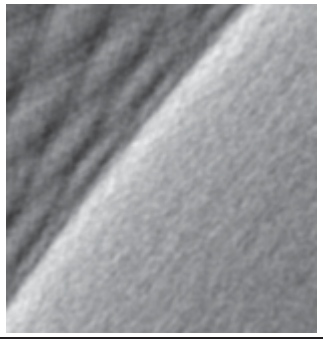
180	22.5	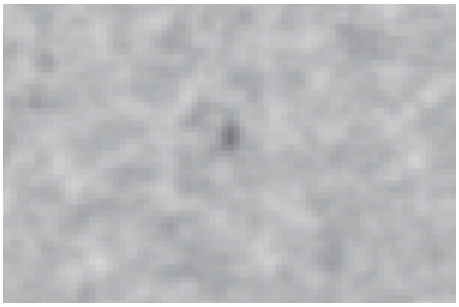	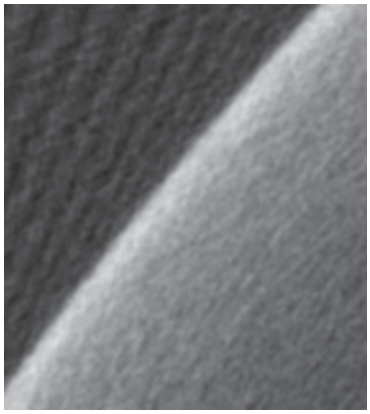

TABLE 12.—CONTINUNED

No. of projection views	SNR	Hole	Wall
360	30.5	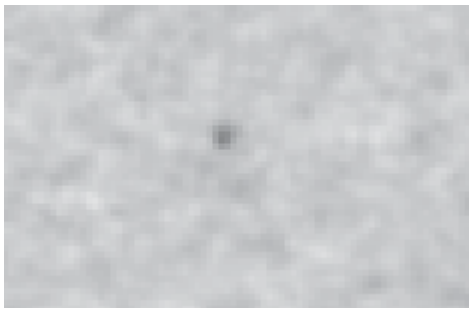	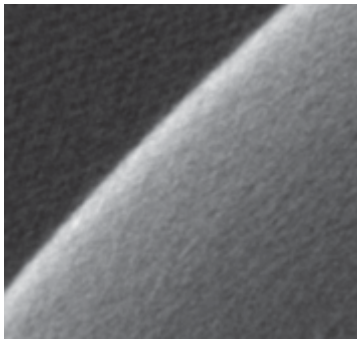
720	39.5		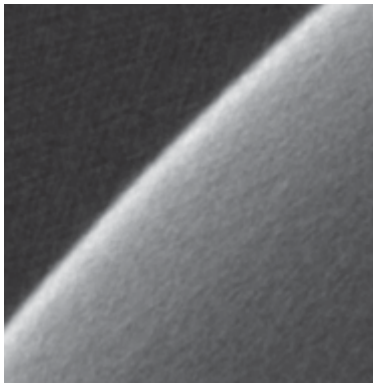
1080	48	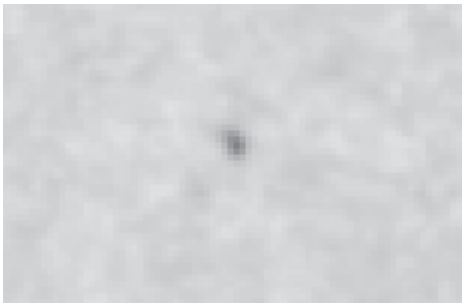	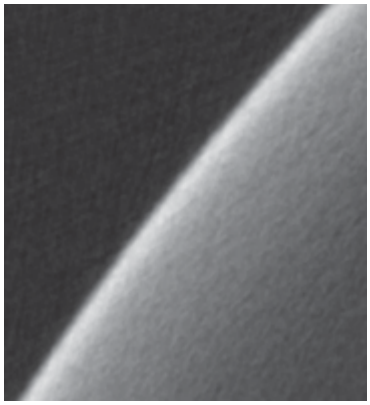
1440	48		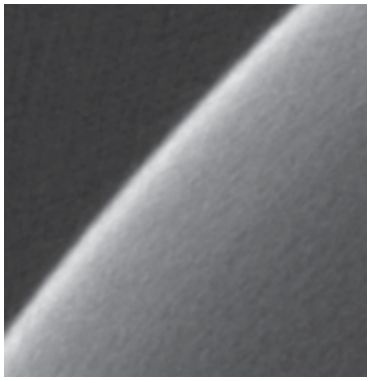

TABLE 12.—CONCLUDED

No. of projection views	SNR	Hole	Wall
1800	48		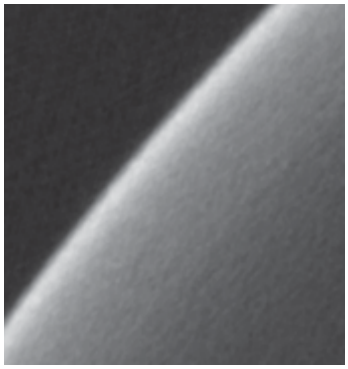
3600	65		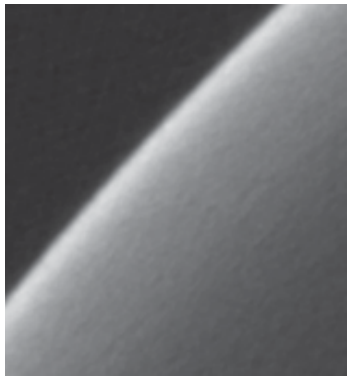

Varying Binning (Transmission Tube)

SNR increases (averaging effect), hole detectability decreases, and wall / features become more pixelated with an increase in binning size. The inner cylinder wall is not resolved at 70 kV voltage but would be expected to exhibit similar pixilation with increased binning for CT scan run at higher voltages such as at 190 kV. For experiment parameters see Table 13 and for results see Table 14.

TABLE 14.—EXPERIMENTAL PARAMETERS FOR EFFECT OF BINNING EXPERIMENTS

Parameter	Value
Binning	1×1, 2×2, 4×4
Voltage, kV	70
Current, μA	200
Estimated approximate focal spot, μm	7
Frame rate, fps	3
Number of frame averages	3
Number of projection views	360
Filtering	0.010 in. Cu
Magnification factor	6.62
Voxel dimension, μm	11.3

TABLE 15.—RESULTS FOR EFFECT OF BINNING

Binning	SNR	Hole	Wall
1×1	30.5	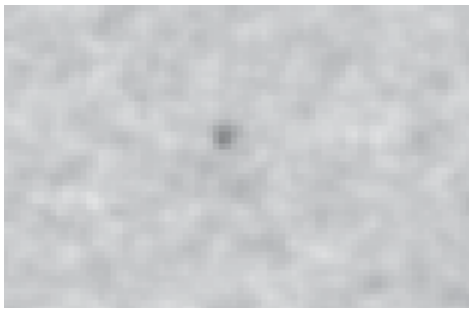	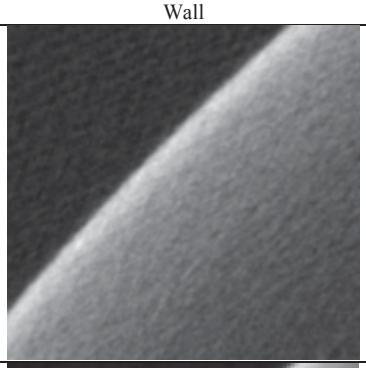
2×2	55		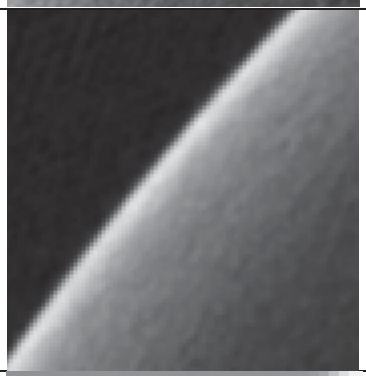
4×4	72.8		

Varying Cylinder Orientation (Transmission Tube)

The wall thickness seen by the x-rays through the cylinder walls would slightly increase with tilt and therefore a lower photon flux would be expected leading to a lower SNR (see Table 15 for experiment parameters). It is likely that photon flux varied between experiments causing the unexpected result. The hole was equally detectable at both angles. The outer cylinder wall was sharply defined for both angles and the inner cylinder wall is not resolved at 70 kV voltage in either case (see Table 16). It is expected that inner wall sharpness might be affected over a range of tilt angles from 0° to 45° for CT scans run at higher voltages such as at 190 kV. The series of holes in the reslice image are tilted as shown in Figure 5 for the 3° tilt.

TABLE 16.—EXPERIMENTAL PARAMETERS FOR EFFECT
OF CYLINDER ORIENTATION EXPERIMENTS

Parameter	Value
Cylinder Orientation, tilt	0°, 3°
Voltage, kV	70
Current, µA	200
Estimated approximate focal spot, µm	7
Binning	1×1
Frame rate, fps	3
Number of frame averages	3
Number of projection views	360
Filtering	0.010 in. Cu
Magnification factor	6.62
Voxel dimension, µm	11.3

TABLE 17.—RESULTS FOR EFFECT OF CYLINDER TILT

Cylinder orientation	SNR	Hole	Wall
0° tilt	30.5	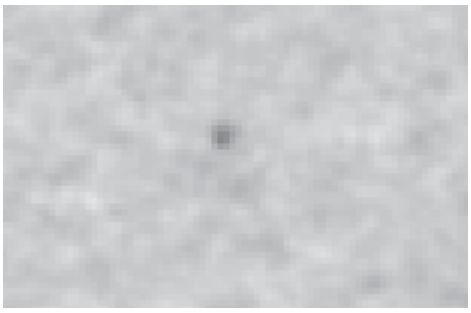	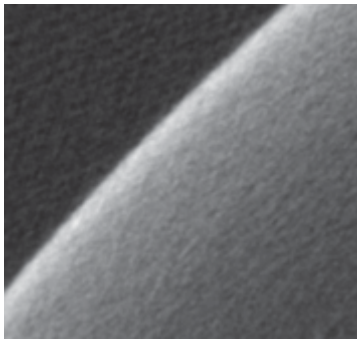
3° tilt	35	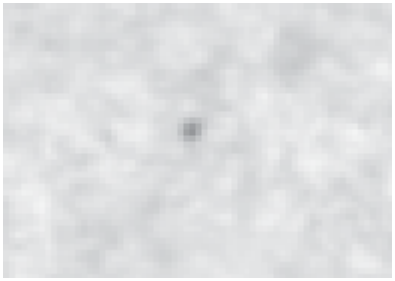	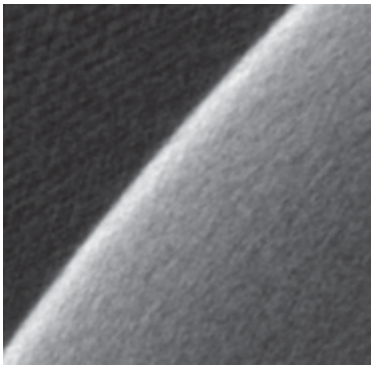

Figure 5.—Sample tilt results in angling of row of holes on the unwrap / reslice image.

Varying Angular Range of Scan (Reflection/Directional Tube)

Gray scale banding (alternating light and dark bands) was apparent in all unwrap reslice images for angle range < 360°. The SNR and hole detectability results do not change in a predictable fashion with a decrease in angle range over which the CT scan was performed. This may indicate that the FDK reconstruction algorithm will show variable results from 180° to 360° (experiment parameters are shown in Table 17). Artifacts and reduced contrast prevail in some cases in the cylinder wall images as angle range is reduced (Table 18). However, the inner wall is reasonably well-resolved in most cases.

TABLE 18.—EXPERIMENTAL PARAMETERS FOR EFFECT OF ANGULAR RANGE OF ACQUISITION EXPERIMENTS

Parameter	Value
Angular range of acquisition	360°, 300°, 270°, 240°, 210°, 180°
Voltage, kV	190
Current, μA	120
Estimated approximate focal spot, μm	10
Binning	1×1
Frame rate, fps	3
Number of frame averages	3
Angular increment	0.2°
Filtering	0.16 in. Cu
Magnification factor	6.62
Voxel dimension, μm	11.3

TABLE 19.—RESULTS FOR EFFECT OF ANGULAR RANGE OF ACQUISITION. UNWRAPPEDRESLICE IMAGE BRIGHTNESS RESULTS VARIED CONSIDERABLY FOR THIS SET OF EXPERIMENTS

Angular range (°)/no. of views	SNR	Hole	Wall
360° / 1800	27.5	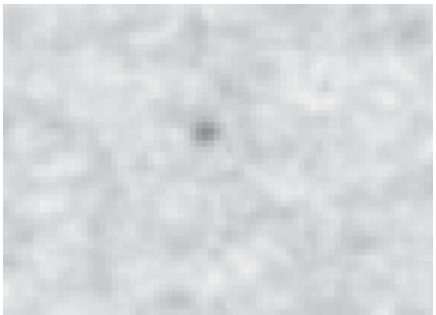	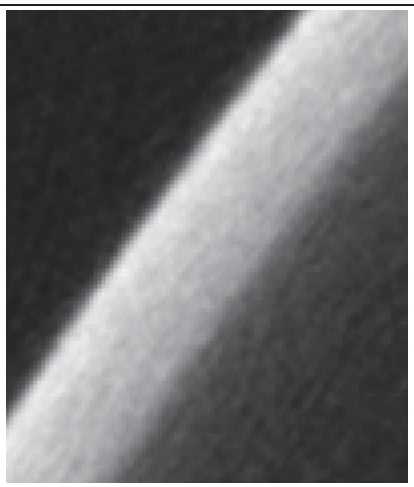

TABLE 20.—CONTINUED

Angular range (°)/no. of views	SNR	Hole	Wall
300° / 1500	25 to 50 (banding)	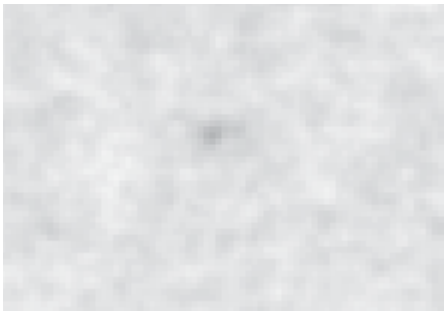	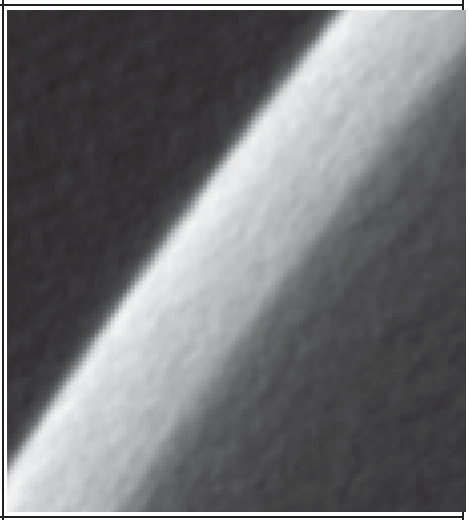
270° / 1350	6 to 13 (banding)	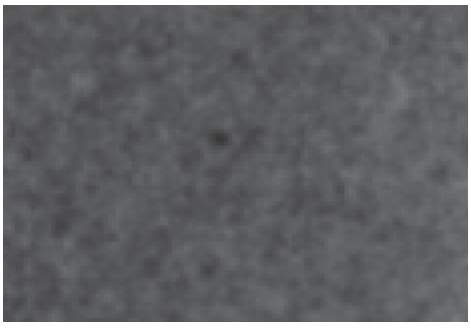	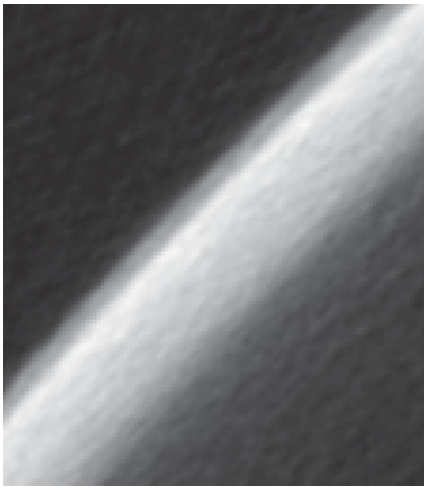
240° / 1200	13 to 28 (banding)	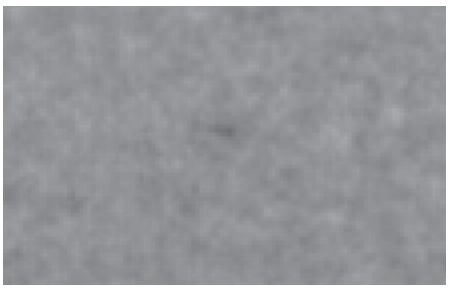	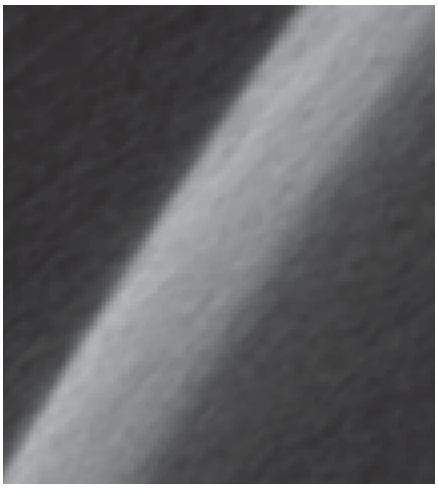

TABLE 21.—CONCLUDED

Angular range (°)/no. of views	SNR	Hole	Wall
210° / 1050	20 to 30 (banding)	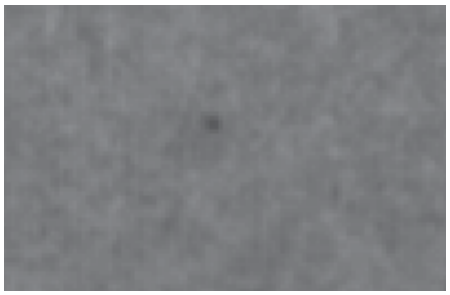	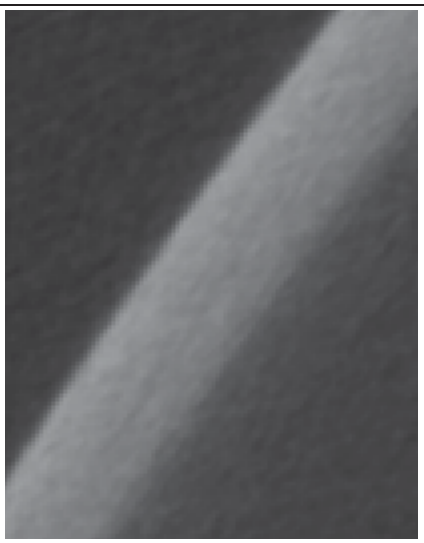
180° / 900	3 to 45 (banding)	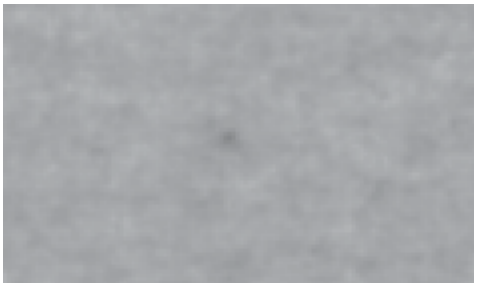	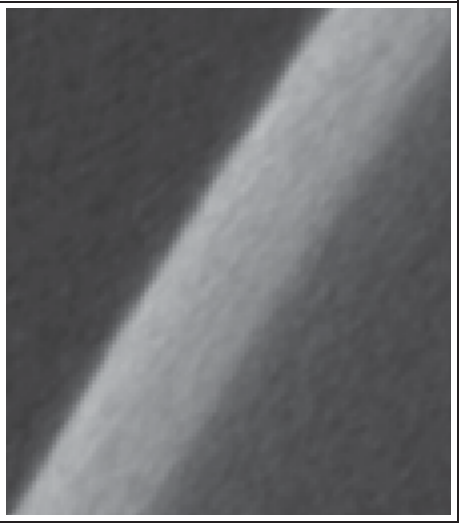

Varying Beam Width and Effective Object Radius (Via Source-to-Object (SO) Distance Variation) (Reflection/Directional Tube)

Effective beam width in the test sample is a function of focal spot size, detector element size, and SO distance (Ref. 7), (see Table 19 for experiment parameters). The further the object from the source, the larger the effective beam width (see Figure 6). The object-to-detector distance will also affect the effective object radius that the detector sees. For objects smaller than the detector and moving them closer to the detector, the x-rays that penetrate the object will impinge on a smaller number of pixels (and a decrease in the effective object radius will result, see Table 20). Photon count reaching the detector, scatter conditions, magnification and geometric unsharpness also change for different SO distances.

SNR did not monotonically increase with increasing SO distance (increasing beam width and decreasing effective object radius) as predicted by Equation (1). SNR was significantly lower at SO = 480 mm than for the other two SO distances, indicating a possible change in scatter conditions. As expected, resolution decreases with increasing SO, as manifested by the hole being more difficult to detect and the cylinder inner wall becoming pixelated.

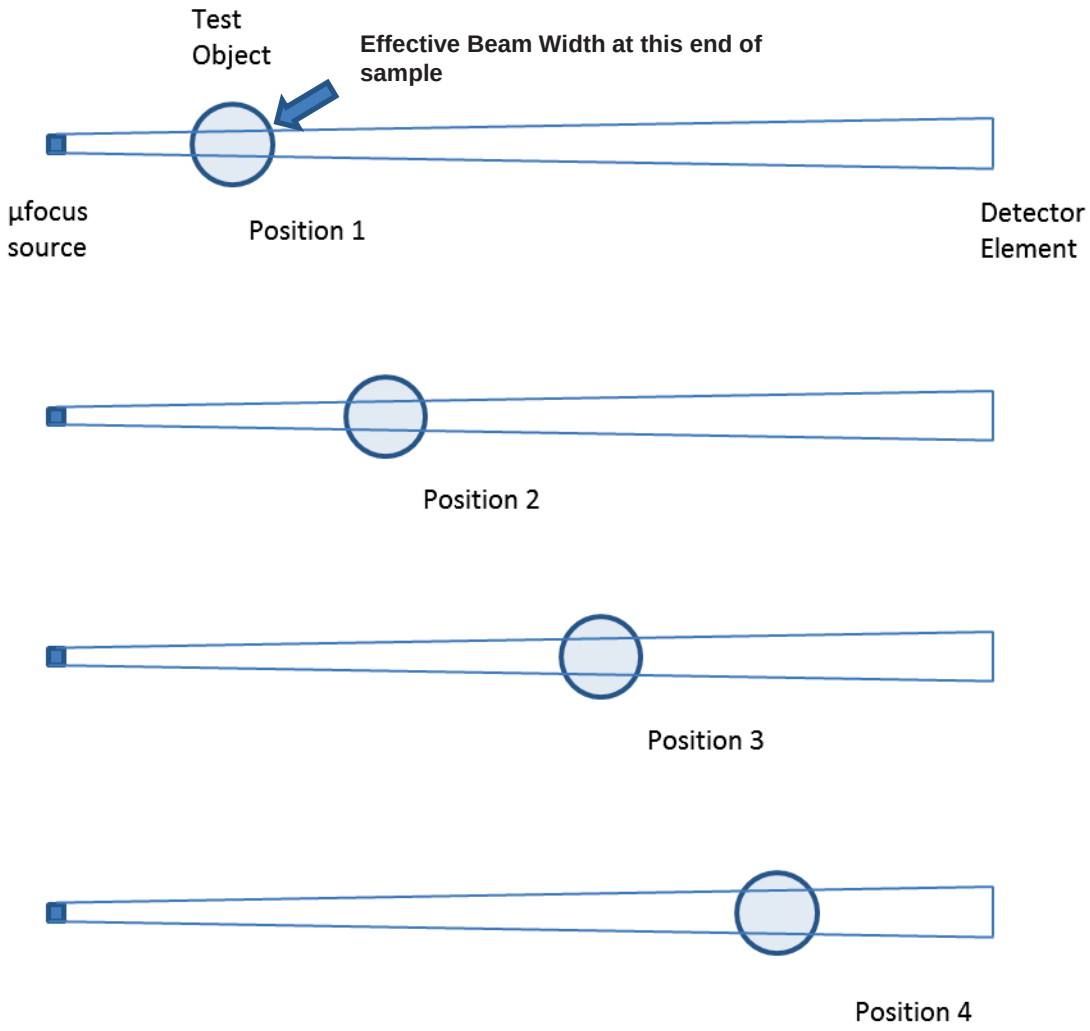

Figure 6.—Effective x-ray beam width in test object as a function of source-to-object position. Focal spot estimated at 7 to 10 µm. Detector pixel element size ~ 75 µm.

TABLE 22.—EXPERIMENTAL PARAMETERS FOR EFFECT OF BEAM WIDTH AND EFFECTIVE OBJECT RADIUS

Parameter	Value
SO distance, mm	120, 240, 480
Voltage, kV	190
Current, µA	120
Estimated approximate focal spot, µm	10
Binning	1×1
Frame rate, fps	3
Number of frame averages	3
Number of projection views	720
Filtering	0.16 in. Cu
Magnification factor	Will vary with SO distance

TABLE 23.—RESULTS FOR EFFECT OF BEAM WIDTH AND EFFECTIVE OBJECT RADIUS (VIA SOURCE-TO-OBJECT (SO) DISTANCE CHANGE)

Beam width/magnification factor/SO	SNR	Hole	Wall
Smallest / 6.7x (SO = 120 mm)	25	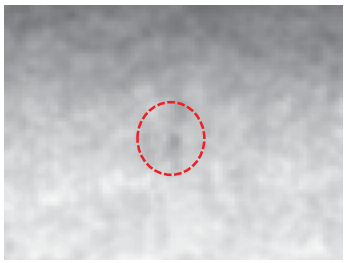	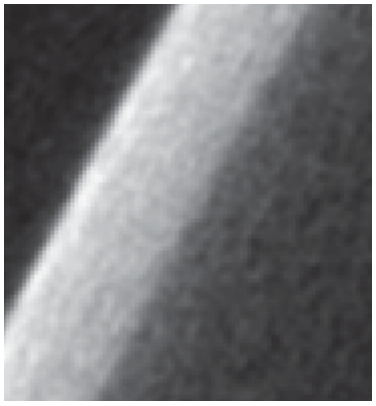
Larger / 3.33x (SO = 240 mm)	28	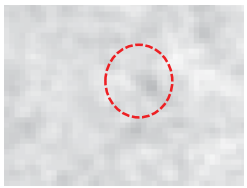 Hole barely detected	
Largest / 1.67x (SO = 480 mm)	18	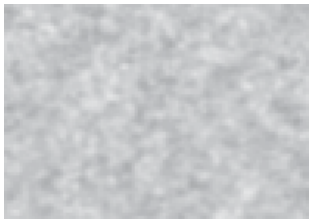 Hole not detected	

Varying Current (Reflection/Directional Tube)

Current directly affects photon count at the detector. The mean counts value with no sample present was approximately 36, 49, and 64 percent of the detector's saturation limit of 16,384 for currents of 80, 120, and 160 μA, respectively (see Table 21 and Table 22).

SNR increased with increasing current as expected from Equation (1). Hole detectability appeared to best at lowest current which may be due to the smaller focal spot at lower power. Hole and wall images appear less noisy which agrees with the increasing SNR measure. The inner cylinder wall appears to be sharper with increasing current.

TABLE 24.—EXPERIMENTAL PARAMETERS
FOR EFFECT OF CURRENT

Parameter	Value
Current, μA	80, 120, 160
Voltage, kV	170
Estimated approximate focal spot, μm	10
Binning	1×1
Frame rate, fps	3
Number of frame averages	3
Number of projection views	720
Filtering	0.16 in. Cu
Magnification factor	6.62

TABLE 25.—RESULTS FOR EFFECT OF CURRENT (AFFECTING PHOTON INTENSITY RATE)

Current, μA	SNR	Hole	Wall
80	16	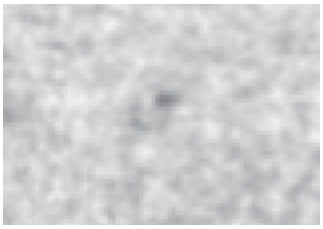	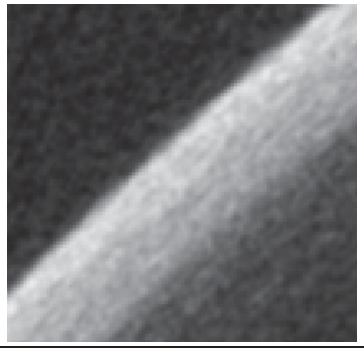
120	22.5		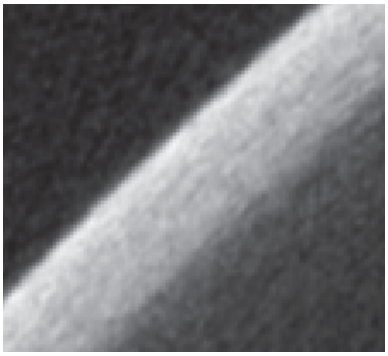
160	28	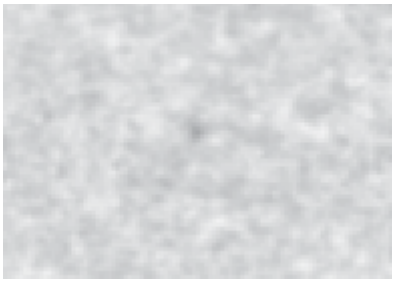	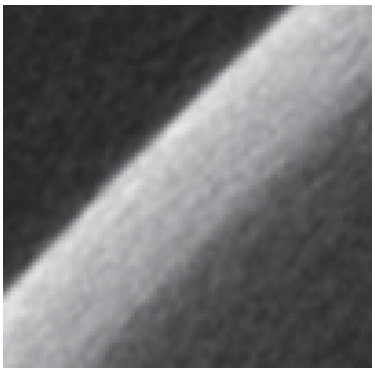

Varying Integration Time (Reflection/Directional Tube)

Frame rate (integration time) directly affects photon count at the detector. The mean counts value with no sample present was approximately 88, 64, and 52 percent of the detector's saturation limit of 16,384 for 2, 3, and 4 fps, respectively (see Table 23 and Table 24).

SNR, hole detectability, and inner cylinder wall visibility increased with increasing integration time (decreasing frame rate) as expected as expected from Equation (1).

TABLE 26.—EXPERIMENTAL PARAMETERS FOR EFFECT OF INTEGRATION TIME (FRAME RATE)

Parameter	Value
Frame rate, fps	2, 3, 4
Voltage, kV	190
Current, μA	120
Estimated approximate focal spot, μm	10
Binning	1×1
Number of frame averages	3
Number of projection views	720
Filtering	0.16 in. Cu
Magnification factor	6.62

TABLE 27.—RESULTS FOR EFFECT OF INTEGRATION TIME (FRAME RATE)

Frame rate	SNR	Hole	Wall
2	25	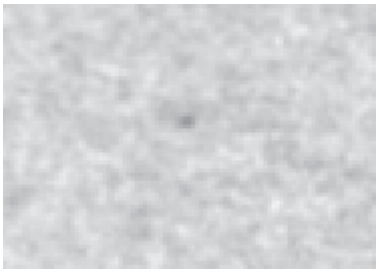	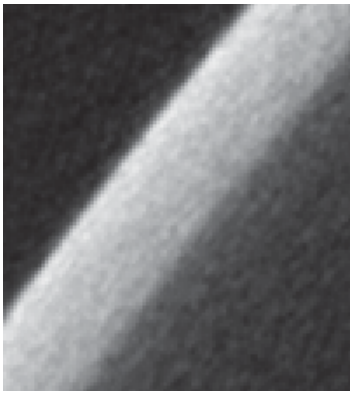
3	23	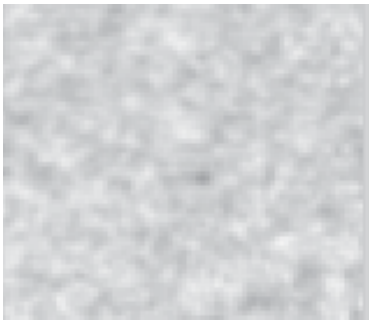	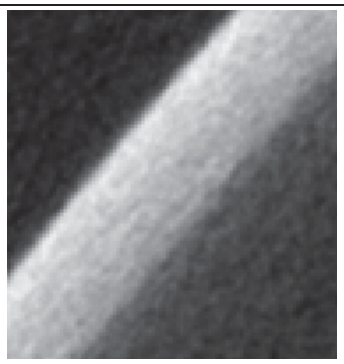
4	20	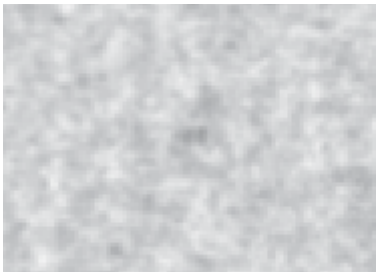	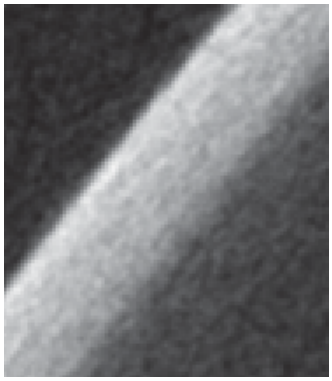

Summary

A study was performed on the effect of experimental variables on radiographic sensitivity (image quality) in x-ray micro-computed tomography images for a high density thin wall metallic cylinder containing micro-EDM holes. Image quality was evaluated in terms of signal-to-noise ratio, flaw detectability, and feature sharpness. The variables included: day-to-day reproducibility, current, integration time, voltage, filtering, number of frame averages, number of projection views, beam width, effective object radius, binning, orientation of sample, angle range (180° to 360°), and directional versus transmission tube. Table 25 to Table 27 provide textual and pictorial summaries of the results of this study.

TABLE 28.—SUMMARY OF STUDY RESULTS

Figure of merit / Variable	SNR	EDM hole detectability	*Inner* cylinder wall sharpness	Comment
Reproducibility (3 trials)	Variable.	Variable.	Reasonably Consistent.	Photon count at detector likely not identical from day-to-day.
Voltage (130, 150, 170, 190, 210 kV)	Variable and not well-defined trend.	Reasonably consistent moderate detectability.	Increase in wall sharpness with increase in voltage.	
Filtering at 210 kV (0.16 in. Cu, 0.24 in. Steel, 0.028 in. Pb)	Reasonably Consistent.	Reasonably consistent moderate detectability.	Reasonably Consistent moderately sharp inner wall.	Hole was less detectable at 210 kV vs. 170 kV indicating poorer contrast at higher voltage.
Filtering at 170 kV (0.16 in. Cu, 0.24 in. Steel, 0.028 in. Pb)	Variable.	Reasonably consistent good detectability.	Ill-defined inner wall except using 0.16 in. Cu Filter.	Hole was more detectable at 170 kV vs. 210 kV indicating better contrast at lower voltage.
Filtering at 130 kV (0.16 in. Cu, 0.24 in. Steel, 0.028 in. Pb)	Variable.	Reasonably consistent good detectability.	Ill-defined.	130 kV too low to resolve inner wall indicating poorer penetration at lower kV.
Number of Frame Averages (1, 3, 5, 9, 15)	Increase in SNR with increase in number of frame averages.	Hole more easily resolved with increase in frame averaging.	Wall not defined at 70 kV regardless of number of frame averages. Based on results for outer wall, inner wall definition likely would increase with increasing number of frame averages for CT scans run at 190 kV.	Outer wall more well-defined with increase in number of frame averages.
Number of Projection Views (9, 18, 36, 90, 180, 360, 720, 1080, 1440, 1800)	Increase in SNR with increase in number of projection views.	Hole less detectable below 360 projection views.	Wall not defined at 70 kV regardless of number of projection views. Based on results for outer wall, inner wall definition likely would increase with increasing number of frame averages for CT scans run at 190 kV.	Outer wall more well-defined with increase in number of projection views.
Beam Width and Effective Object Radius via variation of SO distance	Variable.	Best detectability at smaller beam width and larger effective radius.	Best wall definition at smaller beam width and larger effective radius.	Appears to be an optimal SO distance to achieve best SNR. Features more pixelated with increase in SO distance.
Binning (1x1, 2x2, 4x4)	Increase in SNR with increase in bin size.	Poorer detectability with increase in bin size.	Poorer definition with increase in bin size.	Features more pixelated with increase binning.
Sample Orientation / tilt (0°, 3°)	Variable.	Consistently good detectability over this small tilt range.	Wall not defined at 70 kV. Inner wall sharpness likely would be affected by tilt angles over range 0° to 45° for CT scans run at 190 kV.	Would not expect variation unless tilt significantly changed.
Angle Range of Acquisition (360°, 300°, 270°, 240°, 210°, 180°)	Highly variable.	Variable detectability, not always in predictable fashion.	Variable definition but mostly resolved at all angular ranges of acquisition.	Highly variable SNR within images < 360° angular range of acquisition. Results not predictable.
Directional versus Transmission Tube (Varying Voltage)	Variable for both and not well-defined trend.	Reasonably consistent good detectability.	Increase in wall sharpness with increase in voltage for both tube types.	The inner wall appears to be more highly resolved at most voltages for the reflection tube versus transmission tube. This may be due to a higher respective photon flux at detector during the reflection tube experiments.
Current (80, 120, 160 μA)	Increase in SNR with increase in current.	Lowest current gave best visibility of hole.	Increase in wall sharpness with increase in current.	Would have expected hole detectability results to mimic those of integration time.
Integration Time (2, 3, 4 fps)	Increase in SNR with increase in integration time.	Increase in detectability with increase in integration time.	Increase in wall sharpness with increase in integration time.	

TABLE 29.—PICTORIAL SUMMARY OF STUDY RESULTS FOR HOLE DETECTABILITY

Parameter				
Filter (V = 170 kV)	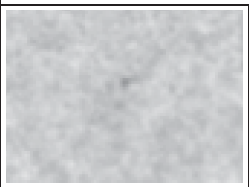 0.16 in. Cu	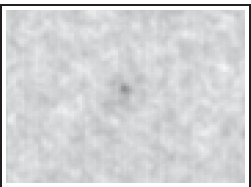 0.24 in. Steel	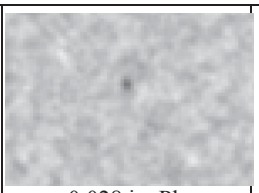 0.028 in. Pb	
Voltage, kV (0.16 in. Cu filter)	210	170	130	
Tube Type (V = 170 kV, 0.16 in. Cu filter)	Transmission	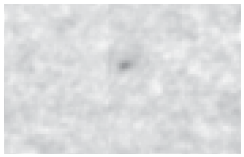 Reflection		
Number of frame averages (V = 70 kV, 0.010 in. Cu filter)	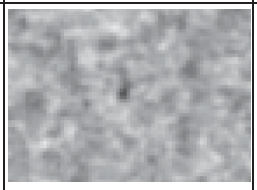 1	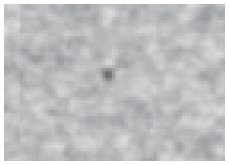 3	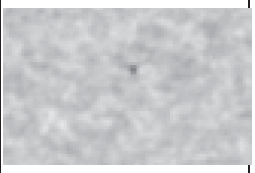 9	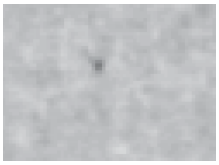 15
Number of projection views (V = 70 kV, 0.010 in. Cu filter)	36	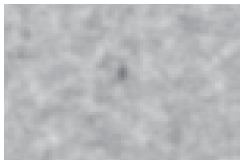 180	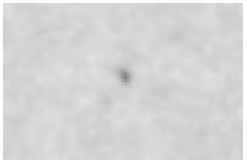 1080	3600
Binning (V = 70 kV, 0.010 in. Cu filter)	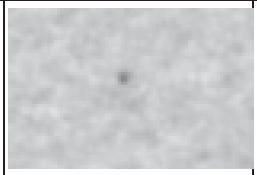 1x1	2x2	4x4	

TABLE 26.—CONCLUDED

Parameter				
Angular range of scan (V = 190 kV, 0.16 in. Cu filter)	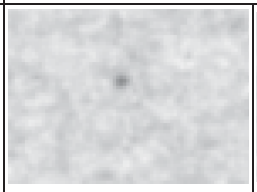 360°	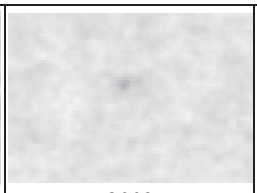 300°	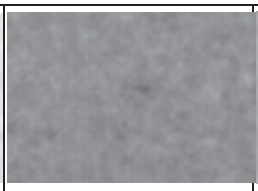 240°	180°
Beam width (V = 190 kV, 0.16 in. Cu filter)	Smallest	Larger	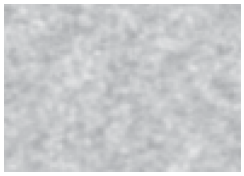 Largest	
Current (μA) (V = 170 kV, 0.16 in. Cu Filter)	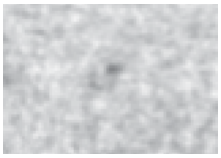 80	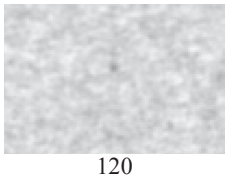 120	160	
Integration time, fps (V = 190 kV, 0.16 in. Cu filter)	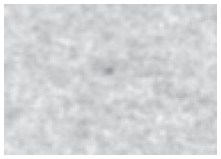 2	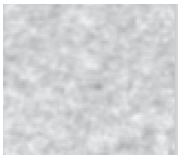 3	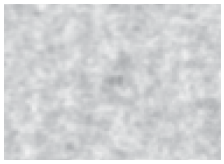 4	

TABLE 30.—PICTORIAL SUMMARY OF STUDY RESULTS FOR INNER WALL SHARPNESS

[Note: Outer wall shown where inner wall was not resolved.]

Parameter				
Filter (V = 170 kV)	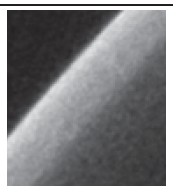 0.16 in. Cu	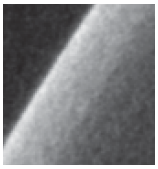 0.24 in. Steel	 0.028 in. Pb	
Voltage, kV (0.16 in. Cu Filter)	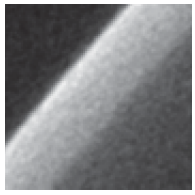 210	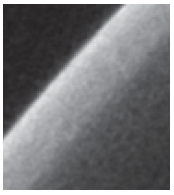 170	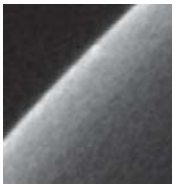 130	
Tube type (V = 170 kV, 0.16 in. Cu filter)	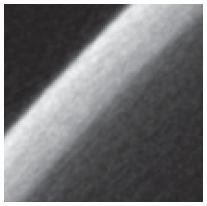 Transmission	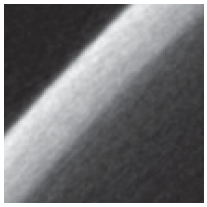 Reflection		
Number of frame averages (V = 70 kV, 0.010 in. Cu Filter)	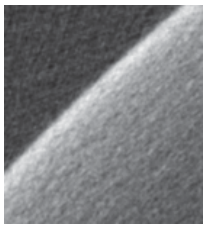 1	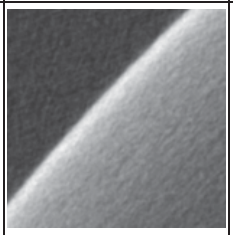 3	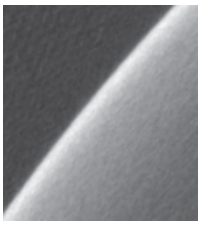 9	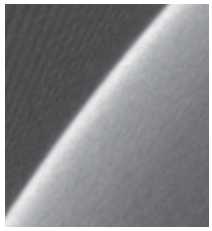 15
Number of projection views (V = 70 kV, 0.010 in. Cu Filter)	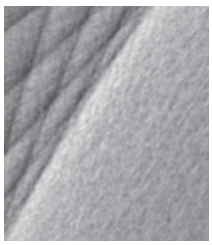 36	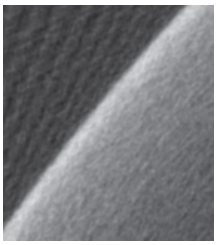 180	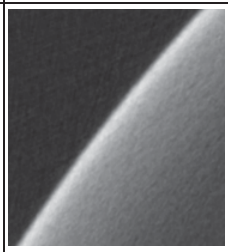 1080	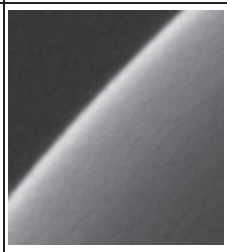 3600

TABLE 31.—CONCLUDED

Parameter				
Binning (V = 70 kV, 0.010 in. Cu filter)	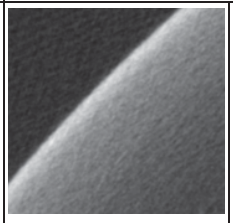 1x1	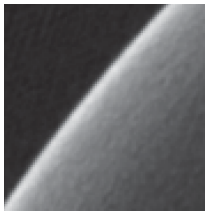 2x2	 4x4	
Angular range of scan (V = 190 kV, 0.16 in. Cu Filter)	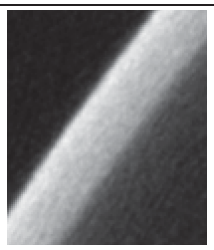 360°	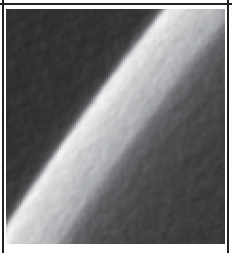 300°	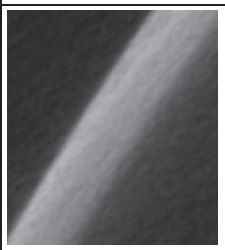 240°	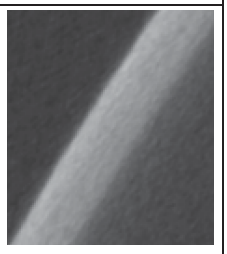 180°
Beam width via SO distance change (V = 190 kV, 0.16 in. Cu Filter)	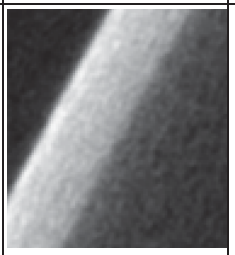 Smallest	 Larger	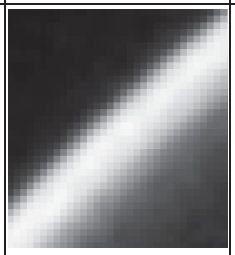 Largest	
Current, μA (V = 170 kV, 0.16 in. Cu Filter)	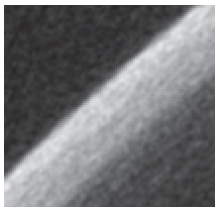 80	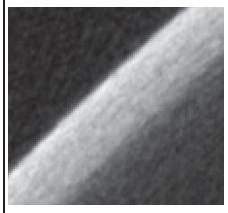 120	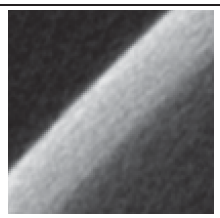 160	
Integration time, fps (V = 190 kV, 0.16 in. Cu Filter)	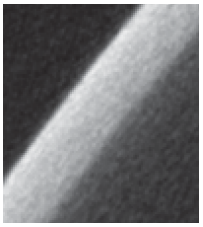 2	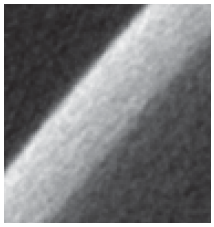 3	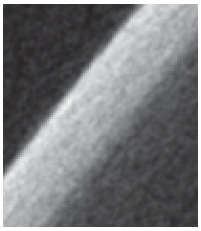 4	

References

1. D. J. Roth, R.W. Rauser, R. R. Bowman, R.E. Martin, A. Koshti, David S. Morgan, "The Critical Role Of High Resolution X-Ray Micro-Computed Tomography For Ultra-Thin Wall Space Component Characterization," Materials Evaluation, March 2014, pp.
2. Richard E. Martin, Don J. Roth, Jon Salem, Application of Advanced Nondestructive Evaluation Techniques for Cylindrical Composite Test Samples, NASA TM-. December, 2013.
3. Ali Abdul-Aziz, D.J. Roth, R. Cotton, George F. Studor, Eric Christiansen, and P.C. Young; "Composite Material Characterization using Microfocus X-ray Computed Tomography Image-based Finite Element Modeling", Materials Evaluation, pp. 167-174, Volume 71, No.2, February 2013
4. Maire, E. and Withers, P.J., "Quantitative X-ray Tomography," International Materials Reviews, Vol. 59, No. 1, pp. 1 – 43, 2014.
5. Howard, P., Portaz, J., Janning, J., Barthelemy, P. and Fauverte, F., "Testing Techniques for High Volume Production Applications," Materials Evaluation, Vol. 68, No. 4, pp. 400–406, April 2010.
6. Barret, H.H. and Swindell, W., Radiological Imaging: The Theory of Image Formation, Detection, and Processing. Vols. 1 and 2. New York, NY: Academic Press (1981).
7. Nondestructive Testing Handbook, Radiographic Testing. Ed. Bossi, R.H., Iddlings, F.A., Wheeler, G.C., and Moore, P.O. Third Ed. Vol. 4. American Society of Nondestructive Testing. pp. 141-142, 313, 316-317, 328 – 338. 2002.
8. MIL-HDBK-1823, Department of Defense Handbook: Nondestructive Evaluation (NDE) System, Reliability Assessment (30 Apr. 1999).
9. Feldkamp, L.A., Davis, L.C., and Kress, J.W., "Practical cone-beam algorithm," J. Opt. Soc. Amer. A6 (1984), 612 – 619.